

CROSSFORMER: A VERSATILE VISION TRANSFORMER BASED ON CROSS-SCALE ATTENTION

Wenxiao Wang^{1,2}, Lu Yao¹, Long Chen³, Deng Cai¹, Xiaofei He¹ & Wei Liu²

¹State Key Lab of CAD & CG, Zhejiang University

²Data Platform, Tencent

³Columbia University

ABSTRACT

Transformers have made much progress in dealing with visual tasks. However, existing vision transformers still do not possess an ability that is important to visual input: building the attention among features of different scales. The reasons for this problem are two-fold: (1) Input embeddings of each layer are equal-scale without cross-scale features; (2) Some vision transformers sacrifice the small-scale features of embeddings to lower the cost of the self-attention module. To make up this defect, we propose **Cross-scale Embedding Layer (CEL)** and **Long Short Distance Attention (LSDA)**. In particular, CEL blends each embedding with multiple patches of different scales, providing the model with cross-scale embeddings. LSDA splits the self-attention module into a short-distance and long-distance one, also lowering the cost but keeping both small-scale and large-scale features in embeddings. Through these two designs, we achieve cross-scale attention. Besides, we propose dynamic position bias for vision transformers to make the popular relative position bias apply to variable-sized images. Based on these proposed modules, we construct our vision architecture called CrossFormer. Experiments show that CrossFormer outperforms other transformers on several representative visual tasks, especially object detection and segmentation. The code has been released: <https://github.com/cheerss/CrossFormer>.

1 INTRODUCTION

Transformer (Vaswani et al., 2017; Devlin et al., 2019; Brown et al., 2020) has achieved great success in natural language processing (NLP). Benefitting from its self-attention module, transformer is born with the ability to build long-distance dependency, and which is also important to many visual tasks. Hence, plenty of researches (Dosovitskiy et al., 2021; Touvron et al., 2021; Wang et al., 2021) have been done to explore transformer-based vision architectures.

Transformer requires a sequence of embeddings (e.g., word embeddings) as input. To adapt it to visual tasks, most existing vision transformers (Dosovitskiy et al., 2021; Touvron et al., 2021; Wang et al., 2021; Liu et al., 2021b) produce embeddings by splitting the image into equal-sized patches. For example, a 224×224 image can be split into 56×56 patches of size 4×4 , and then these patches are projected through a linear layer to become an embedding sequence. Inside the transformer, the self-attention module can build dependencies between any two embeddings. Unfortunately, the memory and computational cost of the vanilla self-attention (Dosovitskiy et al., 2021; Touvron et al., 2021) is too large for visual tasks because the sequence length of visual embeddings is much longer than that of NLP. Thus, many substitutes (Wang et al., 2021; Liu et al., 2021b; Lin et al., 2021) are proposed to approximate the vanilla self-attention module with a lower cost.

Though the works above have made some progress, existing vision transformers still have a problem that restricts their performance — **They fail to build the attentions among features of different scales, while such ability is very important to visual tasks.** For example, an image often contains many objects of different scales, and building the relationships among them requires a cross-scale attention mechanism. Besides, some tasks such as instance segmentation need interactions between large-scale (coarse-grained) features and small-scale (fine-grained) ones. Existing vision transformers fail to deal with these cases because of two reasons: (1) The embedding sequence is generated

from equal-sized patches, so embeddings in the same layer only own features of one single scale. (2) Inside the self-attention module, adjacent embeddings’ *key/value*¹ are often merged (Wang et al., 2021; Chu et al., 2021) to lower the cost. As a result, even if embeddings have both small-scale and large-scale features, merging operations will lose the small-scale (fine-grained) features of every single embedding, thus disabling the cross-scale attention.

To solve this problem, we co-design our embedding layer and self-attention module as follows: (1) *Cross-scale Embedding Layer (CEL)* — Following Wang et al. (2021), we also employ a pyramid structure for our transformer, which naturally splits the model into multiple stages. CEL appears at the start of each stage. It receives last stage’s output (or the image) as input, sampling patches with multiple kernels of different scales (*e.g.*, 4×4 , 8×8 , *etc.*). Then, each embedding is constructed by projecting and concatenating these patches as opposed to using one single-scale patch only. (2) *Long Short Distance Attention (LSDA)* — We also propose a substitute of the vanilla self-attention, but to preserve the small-scale features, embeddings (and neither their *key/value*) will not be merged. In contrast, we split the self-attention module into short-distance attention (SDA) and long-distance attention (LDA). SDA builds the dependencies among neighboring embeddings, while LDA takes charge of dependencies among embeddings far from each other. LSDA also lowers the cost of the self-attention module, but different from others, LSDA does not hurt either small-scale or large-scale features, so attentions with cross-scale interactions are enabled.

Besides, relative position bias (RPB) (Shaw et al., 2018) is an effective position representation for vision transformers. However, it is only applicable when the input image/group size² is fixed, which is not the case for many tasks like object detection. To make it more flexible, we introduce a trainable module called dynamic position bias (DPB), which receives two embeddings’ distance as input and outputs their position bias. The module is optimized end-to-end in the training phase, inducing ignorable cost but making RPB apply to variable image/group size.

Each of our proposed modules can be implemented with about ten lines of code. Based on them, we construct four versatile vision transformers of different sizes called *CrossFormers*. Experiments on four representative visual tasks (*i.e.*, image classification, object detection, and instance/semantic segmentation) show that CrossFormers outperform the previous vision transformers in all these tasks, especially dense prediction tasks (object detection and instance/semantic segmentation). We think it is because image classification only pays attention to one object and large-scale features, while dense prediction tasks rely more on cross-scale attention.

It is worth highlighting our contributions as follows:

- We propose cross-scale embedding layer (CEL) and long short distance attention (LSDA), which compensate for previous architectures’ disability of building cross-scale attention.
- Dynamic position bias module (DPB) is proposed to make the relative position bias more flexible, *i.e.*, applying to variable image size or group size.
- Several CrossFormers of different size are constructed, and we identify their effectiveness through sufficient experiments on four representative visual tasks.

2 BACKGROUND

Vision Transformers. Motivated by transformers for NLP, researchers design visual transformers for vision tasks to take advantage of its great attention mechanism. In particular, ViT (Dosovitskiy et al., 2021) and DeiT (Touvron et al., 2021) transfer the original transformer to visual tasks, achieving impressive accuracy. Later, PVT (Wang et al., 2021), HVT (Pan et al., 2021), Swin (Liu et al., 2021b), *etc.* introduce pyramid structure into transformers, greatly decreasing the number of patches in the later layers of the model. They also extend visual transformers to other tasks like object detection and segmentation (Wang et al., 2021; Liu et al., 2021b).

Self-attention and Its Variants. As the core of transformer, the computational and memory cost of the self-attention module is $O(N^2)$, where N is the length of the embedding sequence. Though such cost is acceptable for image classification, it is not the case for other tasks with much larger input images (*e.g.*, object detection and segmentation). To solve this issue, Swin (Liu et al., 2021b)

¹Input embeddings’ two projections in the self-attention module

²Some vision transformers split input embeddings into several groups. Group size means the number of embeddings in a group.

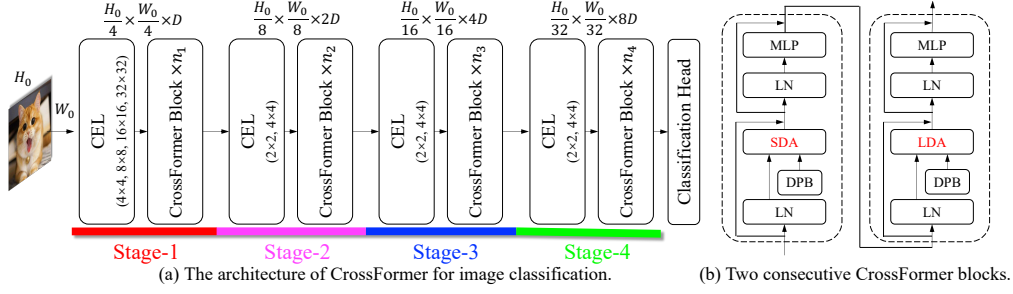


Figure 1: (a) The architecture of CrossFormer for classification. The input size is $H_0 \times W_0$, and the size of feature maps in each stage is shown on the top. Stage- i consists of a CEL and n_i CrossFormer blocks. Numbers in CELs represent the size of used kernels. (b) The inner structure of two consecutive CrossFormer blocks, SDA and LDA appear alternately in different blocks.

restricts the attention in a local region, giving up the long-distance dependency. PVT (Wang et al., 2021) and Twins (Chu et al., 2021) make adjacent embeddings share the same *key/value* to lower the cost. Similarly, other vision transformers (Chen et al., 2021a; Zhang et al., 2021b; Wu et al., 2021) also employ a divide-and-conquer method and approximate the vanilla self-attention at a lower cost.

Position representations. Transformer is combination invariant, that is, shuffling input embeddings does not change the output of the transformer. Nevertheless, the position of embeddings also contains important information. To make the model aware of this, many different position representations of embeddings (Vaswani et al., 2017; Dosovitskiy et al., 2021) are proposed, wherein relative position bias (RPB) (Shaw et al., 2018) is one of them. For RPB, each pair of embeddings has a bias added to their attention, which indicates their relative distance. RPB is shown to be more effective than other position representations for visual tasks in previous works (Liu et al., 2021b; Chen et al., 2021b).

3 CROSSFORMER

The overall architecture of CrossFormer is shown in Figure 1. Following (Wang et al., 2021; Liu et al., 2021b; Lin et al., 2021), CrossFormer also employs a pyramid structure, which naturally splits the model into four stages. Each stage is comprised of a cross-scale embedding layer (CEL, Section 3.1) and several CrossFormer blocks (Section 3.2). The CEL receives last stage’s output (or the image) as input and generates cross-scale embeddings. In this process, CEL (except that in Stage-1) reduces the number of embeddings to a quarter while doubles their dimensions for pyramid structure. Then, several CrossFormer blocks (containing LSDA and DPB) are put after CEL. A specialized head (e.g., the classification head) follows after the final stage for the specific task.

3.1 CROSS-SCALE EMBEDDING LAYER (CEL)

Cross-scale embedding layer is used to generate input embeddings for each stage. Figure 2 takes the first CEL, which is ahead of the Stage-1, as an example. It receives an image as input, sampling patches using four kernels of different size. The strides of four kernels are kept the same so that they generate the same number of embeddings³. As we can see in Figure 2, every four corresponding patches have the same center but different scales. These four patches will be projected and concatenated as one embedding. In practice, the process of sampling and projecting can be implemented through four convolutional layers.

For a cross-scale embedding, one problem is how to set the projected dimension of each scale. Con-

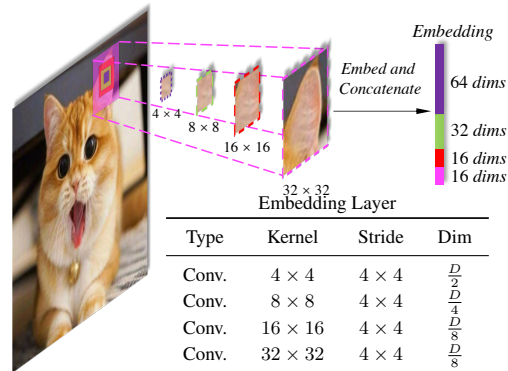


Figure 2: Cross-scale embedding layer (CEL). The input image is sampled by four kernels (i.e., $4 \times 4, 8 \times 8, 16 \times 16, 32 \times 32$) with stride 4×4 . Each embedding is constructed by projecting and concatenating the four patches.

³The image will be padded if necessary

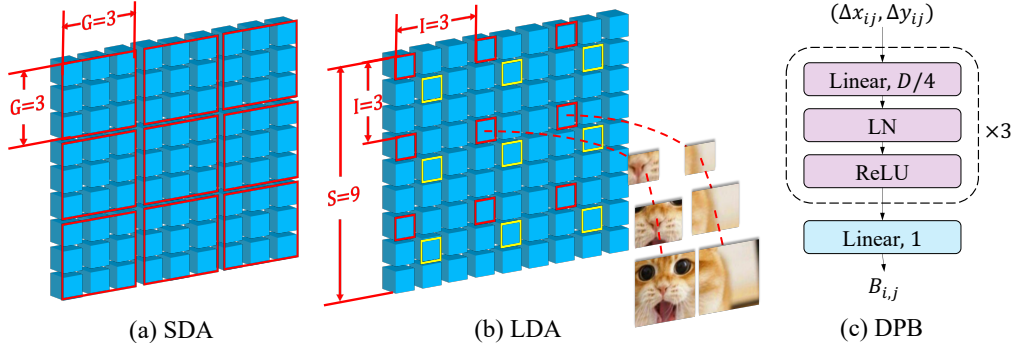


Figure 3: (a) Short distance attention (SDA). Embeddings (blue cubes) are grouped by red boxes. (b) Long distance attention (LDA). Embeddings with the same color borders belong to the same group. Large patches of embeddings in the same group are adjacent. (c) Dynamic position bias (DPB). The dimensions of intermediate layers are $\frac{D}{4}$, and the output is a one-dimensional scalar.

Considering that a large kernel is easier to induce a sizeable computational cost, we use a lower dimension for large kernels while a higher dimension for small kernels. Figure 2 provides the specific allocation rule in its subtable, and a 128 dimensional example is given. Compared with allocating the dimension equally, our scheme saves much computational cost but does not explicitly affect the model’s performance. The cross-scale embedding layers in other stages work in a similar way. As shown in Figure 1, CELs in *Stage-2/3/4* use two kernels (2×2 and 4×4). The strides are set as 2×2 to reduce the number of embeddings to a quarter.

3.2 CROSSFORMER BLOCK

Each CrossFormer block consists of a short-distance attention (SDA) or long-distance attention (LDA) module and a multilayer perceptron (MLP). Especially, as shown in Figure 1b, SDA and LDA appear alternately in different blocks, and dynamic position bias (DPB) works in both SDA and LDA for embeddings’ position representations. Further, residual connection is used in the block.

3.2.1 LONG SHORT DISTANCE ATTENTION (LSDA)

We split the self-attention module into two parts: short-distance attention (SDA) and long-distance attention (LDA). For SDA, every $G \times G$ adjacent embeddings are grouped together. Figure 3a gives an example when $G = 3$. As for LDA with input of size $S \times S$, the embeddings are sampled with fixed interval I . For example, in Figure 3b ($I = 3$), all embeddings with red border belong to a group, and those with yellow border comprise another group. The group’s height/width for LDA is computed as $G = \frac{S}{I}$, and $G = 3$ in this example. After grouping the embeddings, both SDA and LDA employ the vanilla self-attention module within each group. As a result, the memory and computational cost of the self-attention module is reduced from $O(S^4)$ to $O(S^2G^2)$.

In Figure 3b, we draw the component patches of two embeddings. As we can see, the small-scale patches of two embeddings are nonadjacent, and it is difficult to judge their relationship without the help of large-scale patches. Thus, it will be hard to build the dependency between these two embeddings if they are only constructed by small-scale patches. On the contrary, adjacent large-scale patches provide sufficient context to link these two embeddings. As a result, long-distance cross-scale attention becomes easier and more meaningful under the guide of large-scale patches.

We provide the pseudo-code of LSDA in the appendix (A.1). Based on the vanilla multi-head self-attention, LSDA can be implemented with only ten lines of code. Further, only *reshape* and *permute* operations are used, inducing no extra computational cost.

3.2.2 DYNAMIC POSITION BIAS (DPB)

Relative position bias (RPB) indicates embeddings’ relative position by adding a bias to their attention. Formally, the LSDA’s attention map with RPB becomes:

$$Attention = Softmax(QK^T / \sqrt{d} + B)V, \quad (1)$$

Table 1: Variants of CrossFormer for image classification. The example input size is 224×224 . D and H mean embedding dimension and the number of heads in the multi-head self-attention module, respectively. G and I are group size and interval for SDA and LDA, respectively.

	Output Size	Layer Name	CrossFormer-T	CrossFormer-S	CrossFormer-B	CrossFormer-L
Stage-1	56×56 ($S_1 = 56$)	Cross Embed.	Kernel size: $4 \times 4, 8 \times 8, 16 \times 16, 32 \times 32$, Stride=4			
		SDA/LDA MLP	$\begin{bmatrix} D_1 = 64 \\ H_1 = 2 \\ G_1 = 7 \\ I_1 = 8 \end{bmatrix} \times 1$	$\begin{bmatrix} D_1 = 96 \\ H_1 = 3 \\ G_1 = 7 \\ I_1 = 8 \end{bmatrix} \times 2$	$\begin{bmatrix} D_1 = 96 \\ H_1 = 3 \\ G_1 = 7 \\ I_1 = 8 \end{bmatrix} \times 2$	$\begin{bmatrix} D_1 = 128 \\ H_1 = 4 \\ G_1 = 7 \\ I_1 = 8 \end{bmatrix} \times 2$
Stage-2	28×28 ($S_2 = 28$)	Cross Embed.	Kernel size: $2 \times 2, 4 \times 4$, Stride=2			
		SDA/LDA MLP	$\begin{bmatrix} D_2 = 128 \\ H_2 = 4 \\ G_2 = 7 \\ I_2 = 4 \end{bmatrix} \times 1$	$\begin{bmatrix} D_2 = 192 \\ H_2 = 6 \\ G_2 = 7 \\ I_2 = 4 \end{bmatrix} \times 2$	$\begin{bmatrix} D_2 = 192 \\ H_2 = 6 \\ G_2 = 7 \\ I_2 = 4 \end{bmatrix} \times 2$	$\begin{bmatrix} D_2 = 256 \\ H_2 = 8 \\ G_2 = 7 \\ I_2 = 4 \end{bmatrix} \times 2$
Stage-3	14×14 ($S_3 = 14$)	Cross Embed.	Kernel size: $2 \times 2, 4 \times 4$, Stride=2			
		SDA/LDA MLP	$\begin{bmatrix} D_3 = 256 \\ H_3 = 8 \\ G_3 = 7 \\ I_3 = 2 \end{bmatrix} \times 8$	$\begin{bmatrix} D_3 = 384 \\ H_3 = 12 \\ G_3 = 7 \\ I_3 = 2 \end{bmatrix} \times 6$	$\begin{bmatrix} D_3 = 384 \\ H_3 = 12 \\ G_3 = 7 \\ I_3 = 2 \end{bmatrix} \times 18$	$\begin{bmatrix} D_3 = 512 \\ H_3 = 16 \\ G_3 = 7 \\ I_3 = 2 \end{bmatrix} \times 18$
Stage-4	7×7 ($S_4 = 7$)	Cross Embed.	Kernel size: $2 \times 2, 4 \times 4$, Stride=2			
		SDA/LDA MLP	$\begin{bmatrix} D_4 = 512 \\ H_4 = 16 \\ G_4 = 7 \\ I_4 = 1 \end{bmatrix} \times 6$	$\begin{bmatrix} D_4 = 768 \\ H_4 = 24 \\ G_4 = 7 \\ I_4 = 1 \end{bmatrix} \times 2$	$\begin{bmatrix} D_4 = 768 \\ H_4 = 24 \\ G_4 = 7 \\ I_4 = 1 \end{bmatrix} \times 2$	$\begin{bmatrix} D_4 = 1024 \\ H_4 = 32 \\ G_4 = 7 \\ I_4 = 1 \end{bmatrix} \times 2$
Head	1×1	Avg Pooling	Kernel size: 7×7			
		Linear	Classes: 1000			

where $\mathbf{Q}, \mathbf{K}, \mathbf{V} \in \mathbb{R}^{G^2 \times D}$ represent *query*, *key*, *value* in the self-attention module, respectively, and \sqrt{d} is a constant normalizer. $\mathbf{B} \in \mathbb{R}^{G^2 \times G^2}$ is the RPB matrix. In previous works (Liu et al., 2021b), $\mathbf{B}_{i,j} = \hat{\mathbf{B}}_{\Delta x_{ij}, \Delta y_{ij}}$, where $\hat{\mathbf{B}}$ is a fixed-sized matrix, and $(\Delta x_{ij}, \Delta y_{ij})$ is the coordinate distance between i_{th} and j_{th} embeddings. It is obvious that the image/group size is restricted in case that $(\Delta x_{ij}, \Delta y_{ij})$ exceeds the size of $\hat{\mathbf{B}}$. In contrast, we propose an MLP-based module called DPB to generate relative position bias dynamically, *i.e.*,

$$\mathbf{B}_{i,j} = \text{DPB}(\Delta x_{ij}, \Delta y_{ij}). \quad (2)$$

The structure of DPB is shown in Figure 3c. Its non-linear transformation consists of three fully-connected layers with layer normalization (Ba et al., 2016) and ReLU (Nair & Hinton, 2010). The input dimension of DPB is 2, *i.e.*, $(\Delta x_{ij}, \Delta y_{ij})$, and intermediate layers' dimension is set as $\frac{D}{4}$, where D is the dimension of embeddings. DPB is a trainable module optimized along with the whole model. It can deal with any image/group size without worrying about the bound of $(\Delta x_{ij}, \Delta y_{ij})$.

In the appendix (A.2), we prove that DPB is equivalent to relative position bias if the image/group size is fixed. In this case, we can transform a trained DPB to relative position bias in the test phase. We also provide an efficient $O(G^2)$ implementation of DPB when image/group size is variable (the complexity is $O(G^4)$ in the normal case because $\mathbf{B} \in \mathbb{R}^{G^2 \times G^2}$).

Variants of CrossFormer. Table 1 lists the detailed configurations of CrossFormer's four variants (-T, -S, -B, and -L for tiny, small, base, and large, respectively) for image classification. To reuse the pre-trained weights, models for other tasks employ the same backbones as classification except that they may use different G and I . Specifically, besides the configurations same to classification, we also test with $G_1 = G_2 = 14, I_1 = 16$, and $I_2 = 8$ for the detection/segmentation models' first two stages to adapt to larger images. The specific architectures are put in the appendix (A.3). Notably, group size (*i.e.*, G and I) does not affect the shape of weight tensors, so backbones pre-trained on ImageNet can be fine-tuned directly on other tasks even if they use different (G, I) .

4 EXPERIMENTS

Experiments are done on image classification, object detection, instance segmentation, and semantic segmentation. For a fair comparison, we keep the same data augmentation and training settings to other vision transformers as far as possible. The compared algorithms are all competitive vision transformers, including DeiT (Touvron et al., 2021), PVT (Wang et al., 2021), T2T-ViT (Yuan et al., 2021), TNT (Han et al., 2021), CViT (Chen et al., 2021a), Twins (Chu et al., 2021), Swin (Liu et al.,

Table 2: Results on ImageNet validation set. The input size is 224×224 for most models, while is 384×384 for the model with a \dagger . Results of other architectures are drawn from their papers.

Architectures	#Params	FLOPs	Acc.	Architectures	#Params	FLOPs	Acc.
PVT-S	24.5M	3.8G	79.8%	BoTNet-S1-59	33.5M	7.3G	81.7%
RegionViT-T	13.8M	2.4G	80.4%	PVT-L	61.4M	9.8G	81.7%
Twins-SVT-S	24.0M	2.8G	81.3%	DeiT-B	86.0M	17.5G	81.8%
CrossFormer-T	27.8M	2.9G	81.5%	CvT-21	32.0M	7.1G	82.5%
DeiT-S	22.1M	4.6G	79.8%	CAT-B	52.0M	8.9G	82.8%
T2T-ViT	21.5M	5.2G	80.7%	Swin-S	50.0M	8.7G	83.0%
CViT-S	26.7M	5.6G	81.0%	RegionViT-M	41.2M	7.4G	83.1%
PVT-M	44.2M	6.7G	81.2%	Twins-SVT-B	56.0M	8.3G	83.1%
TNT-S	23.8M	5.2G	81.3%	NesT-S	38.0M	10.4G	83.3%
Swin-T	29.0M	4.5G	81.3%	CrossFormer-B	52.0M	9.2G	83.4%
NesT-T	17.0M	5.8G	81.5%	DeiT-B †	86.0M	55.4G	83.1%
CvT-13	20.0M	4.5G	81.6%	ViL-B	55.7M	13.4G	83.2%
ResT	30.2M	4.3G	81.6%	RegionViT-B	72.0M	13.3G	83.3%
CAT-S	37.0M	5.9G	81.8%	Twins-SVT-L	99.2M	14.8G	83.3%
ViL-S	24.6M	4.9G	81.8%	Swin-B	88.0M	15.4G	83.3%
RegionViT-S	30.6M	5.3G	82.5%	NesT-B	68.0M	17.9G	83.8%
CrossFormer-S	30.7M	4.9G	82.5%	CrossFormer-L	92.0M	16.1G	84.0%

2021b), NesT (Zhang et al., 2021b), CvT (Wu et al., 2021), CAT (Lin et al., 2021), ViL (Zhang et al., 2021a), ResT (Zhang & Yang, 2021), TransCNN (Liu et al., 2021a), Shuffle (Huang et al., 2021), BoTNet (Srinivas et al., 2021), and RegionViT (Chen et al., 2021b).

4.1 IMAGE CLASSIFICATION

Experimental Settings. Experiments on classification are done with ImageNet (Russakovsky et al., 2015) dataset. Models are trained on 1.28M training images and tested on 50K validation images. The same training settings as other vision transformers are employed. In particular, we use an AdamW (Kingma & Ba, 2015) optimizer training for 300 epochs with a cosine decay learning rate scheduler, and 20 epochs of linear warm-up are used. The batch size is 1024 split on 8 V100 GPUs. An initial learning rate of 0.001 and a weight decay of 0.05 are used. Besides, we use drop path rate of 0.1, 0.2, 0.3, 0.5 for CrossFormer-T, CrossFormer-S, CrossFormer-B, CrossFormer-L, respectively. Further, Similar to Swin (Liu et al., 2021b), RandAugment (Cubuk et al., 2020), Mixup (Zhang et al., 2018), Cutmix (Yun et al., 2019), random erasing (Zhong et al., 2020), and stochastic depth (Huang et al., 2016) are used for data augmentation.

Results. The results are shown in Table 2. As we can see, CrossFormer achieves the highest accuracy with similar parameters and FLOPs to others. Especially, compared with popular DeiT (Touvron et al., 2021), PVT (Wang et al., 2021), and Swin (Liu et al., 2021b), we outperform them at least 1.2% in accuracy on small models. Further, though RegionViT achieves the same accuracy (82.5%) to us on a small model, it is 0.7% (84.0% vs. 83.3%) lower than us on a large model.

4.2 OBJECT DETECTION AND INSTANCE SEGMENTATION

Experimental Settings. Experiments on object detection and instance segmentation are both done with COCO 2017 dataset (Lin et al., 2014), which contains 118K training and 5K validation images. We use MMDetection-based (Chen et al., 2019) RetinaNet (Lin et al., 2020) and Mask-RCNN (He et al., 2017) as the object detection or instance segmentation head. For both tasks, backbones are initialized with weights pre-trained on ImageNet. The detection/segmentation models are trained with batch size 16 on 8 V100 GPUs, and an AdamW optimizer with an initial learning rate of 1×10^{-4} is used. Following previous works, we adopt $1 \times$ training schedule, *i.e.*, the models are trained for 12 epochs, and images are resized to 800 pixels for the short side.

Results. Results are put in Table 3. As we can see, the second-placed architecture changes along with the experiment, that is, these architectures may perform well in one task but poorly in another task. In contrast, we outperform all others on both tasks (detection and segmentation) and both

Table 3: Object detection and instance segmentation results on COCO *val* 2017. Results for Swin (Liu et al., 2021b) are drawn from Twins (Chu et al., 2021) as Swin does not report results on RetinaNet and Mask-RCNN. Results in blue fonts are the second-placed one. CrossFormers with \ddagger use different group size from classification models, as described in the appendix (A.3).

Method	Backbone	#Params	FLOPs	AP ^b	AP ₅₀ ^b	AP ₇₅ ^b	AP _S ^b	AP _M ^b	AP _L ^b
RetinaNet 1× schedule	ResNet-50	37.7M	234.0G	36.3	55.3	38.6	19.3	40.0	48.8
	CAT-B	62.0M	337.0G	41.4	62.9	43.8	24.9	44.6	55.2
	Swin-T	38.5M	245.0G	41.5	62.1	44.2	25.1	44.9	55.5
	PVT-M	53.9M	—	41.9	63.1	44.3	25.0	44.9	57.6
	ViL-M	50.8M	338.9G	42.9	64.0	45.4	27.0	46.1	57.2
	RegionViT-B	83.4M	308.9G	43.3	65.2	46.4	29.2	46.4	57.0
	TransCNN-B	36.5M	—	43.4	64.2	46.5	27.0	47.4	56.7
	CrossFormer-S	40.8M	282.0G	44.4(+1.0)	65.8	47.4	28.2	48.4	59.4
	CrossFormer-S[‡]	40.8M	272.1G	44.2(+0.8)	65.7	47.2	28.0	48.0	59.1
	ResNet101	56.7M	315.0G	38.5	57.8	41.2	21.4	42.6	51.1
	PVT-L	71.1M	345.0G	42.6	63.7	45.4	25.8	46.0	58.4
	Twins-SVT-B	67.0M	322.0G	44.4	66.7	48.1	28.5	48.9	60.6
	RegionViT-B+	84.5M	328.2G	44.6	66.4	47.6	29.6	47.6	59.0
	Swin-B	98.4M	477.0G	44.7	65.9	49.2	—	—	—
	Twins-SVT-L	110.9M	455.0G	44.8	66.1	48.1	28.4	48.3	60.1
	CrossFormer-B	62.1M	389.0G	46.2(+1.4)	67.8	49.5	30.1	49.9	61.8
	CrossFormer-B[‡]	62.1M	379.1G	46.1(+1.3)	67.7	49.0	29.5	49.9	61.5
Method	Backbone	#Params	FLOPs	AP ^b	AP ₅₀ ^b	AP ₇₅ ^b	AP ^m	AP ₅₀ ^m	AP ₇₅ ^m
Mask-RCNN 1× schedule	PVT-M	63.9M	—	42.0	64.4	45.6	39.0	61.6	42
	Swin-T	47.8M	264.0G	42.2	64.6	46.2	39.1	61.6	42.0
	Twins-PCPVT-S	44.3M	245.0G	42.9	65.8	47.1	40.0	62.7	42.9
	TransCNN-B	46.4M	—	44.0	66.4	48.5	40.2	63.3	43.2
	ViL-M	60.1M	261.1G	43.3	65.9	47.0	39.7	62.8	42.0
	RegionViT-B	92.2M	287.9G	43.5	66.7	47.4	40.1	63.4	43.0
	RegionViT-B+	93.2M	307.1G	44.5	67.6	48.7	41.0	64.4	43.9
	CrossFormer-S	50.2M	301.0G	45.4(+0.9)	68.0	49.7	41.4(+0.4)	64.8	44.6
	CrossFormer-S[‡]	50.2M	291.1G	45.0(+0.5)	67.9	49.1	41.2(+0.2)	64.6	44.3
	CAT-B	71.0M	356.0G	41.8	65.4	45.2	38.7	62.3	41.4
	PVT-L	81.0M	364.0G	42.9	65.0	46.6	39.5	61.9	42.5
	Twins-SVT-B	76.3M	340.0G	45.1	67.0	49.4	41.1	64.1	44.4
	ViL-B	76.1M	365.1G	45.1	67.2	49.3	41.0	64.3	44.2
	Twins-SVT-L	119.7M	474.0G	45.2	67.5	49.4	41.2	64.5	44.5
	Swin-S	69.1M	354.0G	44.8	66.6	48.9	40.9	63.4	44.2
	Swin-B	107.2M	496.0G	45.5	—	—	41.3	—	—
	CrossFormer-B	71.5M	407.9G	47.2(+1.7)	69.9	51.8	42.7(+1.4)	66.6	46.2
	CrossFormer-B[‡]	71.5M	398.1G	47.1(+1.6)	69.9	52.0	42.7(+1.4)	66.5	46.1

model sizes (small and base). Further, CrossFormer’s performance gain over other architectures increases when enlarging the model, indicating that CrossFormer has higher potentials.

4.3 SEMANTIC SEGMENTATION

Experimental Settings. ADE20K (Zhou et al., 2017) is used as the benchmark for semantic segmentation. It covers a broad range of 150 semantic categories, including 20K images for training, and 2K for validation. Similar to models for detection, we initialize the backbone with weights pre-trained on ImageNet, and MMSegmentation-based (Contributors, 2020) semantic FPN and UPerNet (Xiao et al., 2018) are taken as the segmentation head. For FPN (Kirillov et al., 2019), we use an AdamW optimizer with learning rate and weight decay of 1×10^{-4} . Models are trained for 80K iterations with batch size 16. For UPerNet, an AdamW optimizer with an initial learning rate of 6×10^{-5} and a weight decay of 0.01 is used, and models are trained for 160K iterations.

Results. The results are shown in Table 4. Similar to object detection, CrossFormer shows a larger performance gain over others when enlarging the model. For example, CrossFormer-T achieves 1.4% higher IOU than Twins-SVT-B, but CrossFormer-B achieves 3.1% higher IOU than Twins-SVT-L. Besides, CrossFormer shows a more significant advantage over others on dense prediction tasks (*e.g.*, detection and segmentation) than on classification, which indicates that cross-scale interaction in the attention module is more important for dense prediction tasks than for classification.

Table 4: Semantic segmentation results on ADE20K validation set. ‘‘MS IOU’’ means testing with variable input size.

Semantic FPN (80K iterations)				UPerNet (160K iterations)				
Backbone	#Params	FLOPs	IOU	Backbone	#Params	FLOPs	IOU	MS IOU
PVT-M	48.0M	219.0G	41.6	Swin-T	60.0M	945.0G	44.5	45.8
Twins-SVT-B	60.4M	261.0G	45.0	Shuffle-T	60.0M	949.0G	46.6	47.6
Swin-S	53.2M	274.0G	45.2	CrossFormer-S	62.3M	979.5G	47.6(+1.0)	48.4
CrossFormer-S	34.3M	220.7G	46.0(+0.8)	CrossFormer-S[‡]	62.3M	968.5G	47.4(+0.8)	48.2
CrossFormer-S[‡]	34.3M	209.8G	46.4(+1.2)	Swin-S	81.0M	1038.0G	47.6	49.5
PVT-L	65.1M	283.0G	42.1	Shuffle-S	81.0M	1044.0G	48.4	49.6
CAT-B	55.0M	276.0G	43.6	CrossFormer-B	83.6M	1089.7G	49.7(+1.3)	50.6
CrossFormer-B	55.6M	331.0G	47.7(+4.1)	CrossFormer-B[‡]	83.6M	1078.8G	49.2(+0.8)	50.1
CrossFormer-B[‡]	55.6M	320.1G	48.0(+4.4)	Swin-B	121.0M	1088.0G	48.1	49.7
Twins-SVT-L	103.7M	397.0G	45.8	Shuffle-B	121.0M	1096.0G	49.0	—
CrossFormer-L	95.4M	497.0G	48.7(+2.9)	CrossFormer-L	125.5M	1257.8G	50.4(+1.4)	51.4
CrossFormer-L[‡]	95.4M	482.7G	49.1(+3.3)	CrossFormer-L[‡]	125.5M	1243.5G	50.5(+1.5)	51.4

Table 5: Experimental results for ablation study.

(a) Ablation study for cross-scale embedding (CEL) and long short distance attention (LSDA). The base model is CrossFormer-S (82.5%).

PVT-like	Swin-like	LSDA	CEL	Acc.
✓			✓	81.3%
	✓		✓	81.9%
		✓	✓	82.5%
		✓		81.5%

(b) Comparison between different position representations. The base model is CrossFormer-S. Throughput is tested on $1 \times$ V100 GPU.

Method	#Params/FLOPs	Throughput	Acc.
APE	30.9342M/4.9061G	686 imgs/sec	82.1%
RPB	30.6159M/4.9062G	684 imgs/sec	82.5%
DPB	30.6573M/4.9098G	672 imgs/sec	82.5%
DPB-residual	30.6573M/4.9098G	672 imgs/sec	82.4%

4.4 ABLATION STUDIES

Cross-scale Embeddings vs. Single-scale Embeddings. We take experiments by replacing all cross-scale embedding layers with single-scale ones. Single-scale embeddings mean that only one kernel (4×4 for *Stage-1* and 2×2 for other stages) is used for four CELs in the model. Results in Table 5a show that cross-scale embedding gets a great performance gain, *i.e.*, it achieves 0.9% higher accuracy than the model without cross-scale embeddings. More ablation studies about CEL can be seen in the appendix (B.1).

LSDA vs. Other Self-attentions. Two self-attention modules used in PVT and Swin are compared. Specifically, PVT sacrifices the small-scale information when computing the self-attention, while Swin restricts the self-attention in a local region, giving up the long-distance attention. As we can see in Table 5a, compared with PVT- and Swin-like self-attention mechanism, we outperform them at least 0.6% accuracy. The results tell us that performing the self-attention in a long-short distance manner is most conducive to improving the models’ performance.

DPB vs. Other Position Representations. We compare the parameters, FLOPs, throughputs, and accuracy of models among absolute position embedding (APE), relative position bias (RPB), and DPB, and results are shown in Table 5b. DPB-residual means DPB with residual connections. Both DPB and RPB outperform APE for 0.4% accuracy. DPB achieves the same accuracy to RPB with ignorable extra cost, but, as we described in Section 3.2.2, it is more flexible than RPB and applies to variable image size or group size. Further, residual connections in DPB does not help improve the model’s performance (82.5% vs. 82.4%).

5 CONCLUSION

We propose a transformer-based vision architecture called CrossFormer. Its core design includes a cross-scale embedding layer and long-short distance attention (LSDA) module. Further, we propose dynamic position bias (DPB), making the relative position bias apply to any input size. Experiments show that CrossFormer achieves better performance than other vision transformers on several representative vision tasks. Especially, CrossFormer shows improvements in detection and segmentation in a large margin, which indicates that cross-scale embedding and LSDA are particularly essential for dense prediction vision tasks.

A CROSSFORMER

A.1 PSEUDO CODE OF LSDA

The pseudo code for LSDA is shown in Algorithm 1. As we can see, based on the vanilla self-attention module, both SDA and LDA are implemented with only ten lines of code, and only *reshape* and *permute* operations are used.

Algorithm 1 LSDA code (PyTorch-like)

```

# H: height, W: width, G: group size of SDA/LDA
# x: input tensor (H, W, D)
class LSDA():
    def forward(x, type):
        ## group the embeddings
        if type == "SDA":
            x = x.reshape(H // G, G, W // G, G, D).permute(0, 2, 1, 3, 4)
        elif type == "LDA":
            x = x.reshape(G, H // G, G, W // G, D).permute(1, 3, 0, 2, 4)
            x = x.reshape(H * W // (G ** 2), G ** 2, D)

        ## the vanilla self-attention module
        x = Attention(x)

        ## un-group the embeddings
        x = x.reshape(H // G, W // G, G, G, D)
        if type == "SDA":
            x = x.permute(0, 2, 1, 3, 4).reshape(H, W, D)
        elif type == "LDA":
            x = x.permute(2, 0, 3, 1, 4).reshape(H, W, D)
        return x

```

A.2 DYNAMIC POSITION BIAS (DPB)

Figure 4 gives an example of computing $(\Delta x_{ij}, \Delta y_{ij})$ with $G = 5$ in the DPB module. For a group of size $G \times G$, it is easy to deduce that:

$$\begin{aligned}
 0 &\leq x, y < G \\
 1 - G &\leq \Delta x_{ij} \leq G - 1 \\
 1 - G &\leq \Delta y_{ij} \leq G - 1.
 \end{aligned} \tag{3}$$

Thus, motivated by the relative position bias, we construct a matrix $\hat{B} \in \mathbb{R}^{(2G-1) \times (2G-1)}$, where

$$\hat{B}_{i,j} = DPB(1 - G + i, 1 - G + j), \quad 0 \leq i, j < 2G - 1. \tag{4}$$

The complexity of computing \hat{B} is $O(G^2)$. Then, the bias matrix B in DPB can be drawn from \hat{B} , i.e.,

$$B_{i,j} = \hat{B}_{\Delta x_{ij}, \Delta y_{ij}}. \tag{5}$$

When the image/group size (i.e., G) is fixed, both \hat{B} and B will be also unchanged in the test phase. Therefore, we only need to compute \hat{B} and B once, and DPB is equivalent to relative position bias in this case.

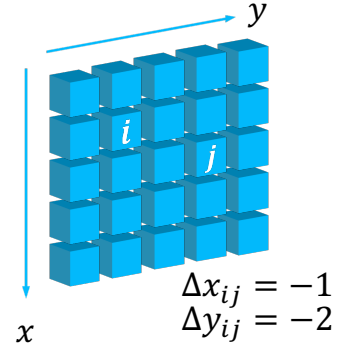


Figure 4: An example of computing $(\Delta x_{ij}, \Delta y_{ij})$.

A.3 VARIANTS OF CROSSFORMER FOR DETECTION AND SEGMENTATION

We test two different backbones for dense prediction tasks. The variants of CrossFormer for dense prediction (object detection, instance segmentation, and semantic segmentation) are in Table 6. The architectures are same to those for image classification except that different G and I in the first two stages are used. Notably, group size (i.e., G and I) does not affect the shape of weight tensors, so backbones pre-trained on ImageNet can be fine-tuned directly on other tasks even if they use different G and I .

Table 6: CrossFormer-based backbones for object detection and semantic/instance segmentation. The example input size is 1280×800 . D and H mean embedding dimension and the number of heads in the multi-head self-attention module, respectively. G and I are group size and interval for SDA and LDA, respectively.

Output Size	Layer Name	CrossFormer-T	CrossFormer-S	CrossFormer-B	CrossFormer-L
Stage-1	Cross Embed.	Kernel size: $4 \times 4, 8 \times 8, 16 \times 16, 32 \times 32$, Stride=4			
	SDA/LDA MLP	$\begin{bmatrix} D_1 = 64 \\ H_1 = 2 \\ G_1 = 14 \\ I_1 = 16 \end{bmatrix} \times 1$	$\begin{bmatrix} D_1 = 96 \\ H_1 = 3 \\ G_1 = 14 \\ I_1 = 16 \end{bmatrix} \times 2$	$\begin{bmatrix} D_1 = 96 \\ H_1 = 3 \\ G_1 = 14 \\ I_1 = 16 \end{bmatrix} \times 2$	$\begin{bmatrix} D_1 = 128 \\ H_1 = 4 \\ G_1 = 14 \\ I_1 = 16 \end{bmatrix} \times 2$
Stage-2	Cross Embed.	Kernel size: $2 \times 2, 4 \times 4$, Stride=2			
	SDA/LDA MLP	$\begin{bmatrix} D_2 = 128 \\ H_2 = 4 \\ G_2 = 14 \\ I_2 = 8 \end{bmatrix} \times 1$	$\begin{bmatrix} D_2 = 192 \\ H_2 = 6 \\ G_2 = 14 \\ I_2 = 8 \end{bmatrix} \times 2$	$\begin{bmatrix} D_2 = 192 \\ H_2 = 6 \\ G_2 = 14 \\ I_2 = 8 \end{bmatrix} \times 2$	$\begin{bmatrix} D_2 = 256 \\ H_2 = 8 \\ G_2 = 14 \\ I_2 = 8 \end{bmatrix} \times 2$
Stage-3	Cross Embed.	Kernel size: $2 \times 2, 4 \times 4$, Stride=2			
	SDA/LDA MLP	$\begin{bmatrix} D_3 = 256 \\ H_3 = 8 \\ G_3 = 7 \\ I_3 = 2 \end{bmatrix} \times 8$	$\begin{bmatrix} D_3 = 384 \\ H_3 = 12 \\ G_3 = 7 \\ I_3 = 2 \end{bmatrix} \times 6$	$\begin{bmatrix} D_3 = 384 \\ H_3 = 12 \\ G_3 = 7 \\ I_3 = 2 \end{bmatrix} \times 18$	$\begin{bmatrix} D_3 = 512 \\ H_3 = 16 \\ G_3 = 7 \\ I_3 = 2 \end{bmatrix} \times 18$
Stage-4	Cross Embed.	Kernel size: $2 \times 2, 4 \times 4$, Stride=2			
	SDA/LDA MLP	$\begin{bmatrix} D_4 = 512 \\ H_4 = 16 \\ G_4 = 7 \\ I_4 = 1 \end{bmatrix} \times 6$	$\begin{bmatrix} D_4 = 768 \\ H_4 = 24 \\ G_4 = 7 \\ I_4 = 1 \end{bmatrix} \times 2$	$\begin{bmatrix} D_4 = 768 \\ H_4 = 24 \\ G_4 = 7 \\ I_4 = 1 \end{bmatrix} \times 2$	$\begin{bmatrix} D_4 = 1024 \\ H_4 = 32 \\ G_4 = 7 \\ I_4 = 1 \end{bmatrix} \times 2$

Table 7: Results on ImageNet validation set. The baseline model is CrossFormer-S (82.5%). We test with different kernel sizes of CELs.

Stage-1	CEL's Kernel Size				#Params	FLOPs	Acc.
	Stage-2	Stage-3	Stage-4				
4×4	2×2	2×2	2×2		28.3M	4.5G	81.5%
8×8	2×2	2×2	2×2		28.3M	4.5G	81.9%
$4 \times 4, 8 \times 8$	$2 \times 2, 4 \times 4$	$2 \times 2, 4 \times 4$	$2 \times 2, 4 \times 4$		30.6M	4.8G	82.3%
$4 \times 4, 8 \times 8, 16 \times 16, 32 \times 32$	$2 \times 2, 4 \times 4$	$2 \times 2, 4 \times 4$	$2 \times 2, 4 \times 4$		30.7M	4.9G	82.5%
$4 \times 4, 8 \times 8, 16 \times 16, 32 \times 32$	$2 \times 2, 4 \times 4, 8 \times 8$	$2 \times 2, 4 \times 4$	2×2		29.4M	5.0G	82.4%

B EXPERIMENTS

B.1 IMAGE CLASSIFICATION.

More experiments are done with different kernel sizes of CELs. As shown in Table 7, simply enlarging the kernel size from 4×4 to 8×8 brings 0.4% accuracy improvement, and cross-scale embeddings achieve the highest performance, they bring at least 0.4% (82.3% vs. 81.9%) performance gain compared with sing-scale embeddings. Further,

B.2 OBJECT DETECTION

Table 8 provides more results on object detection with RetinaNet and Mask-RCNN as detection heads. As we can see, a smaller (G, I) achieves a higher AP than a larger one, but the performance gain is marginal. Considering that a larger (G, I) can save more memory cost, we think $(G_1 = 14, I_1 = 16, G_2 = 14, I_2 = 8)$, which accords with configurations in Table 6, achieves a better trade-off between the performance and cost.

B.3 SEMANTIC SEGMENTATION

Similar to object detection, we test two different configurations of (G, I) for semantic segmentation's backbones. The results are shown in Table 9. As we can see, the memory costs of the two configurations are almost the same, which is different from experiments on object detection. Further, when taking semantic FPN as the detection head, CrossFormers[†] show advantages over CrossForm-

Table 8: Object detection results on COCO val 2017. “Memory” means the allocated memory per GPU reported by `torch.cuda.max_memory_allocated()`. [‡] indicates that models use different (G, I) from classification models.

Method	Backbone	G_1	I_1	G_2	I_2	Memory	#Params	FLOPs	AP ^b	AP ₅₀ ^b	AP ₇₅ ^b
RetinaNet 1× schedule	CrossFormer-S	7	8	7	4	14.7G	40.8M	282.0G	44.4	65.8	47.4
	CrossFormer-S [‡]	14	16	14	8	11.9G	40.8M	272.1G	44.2	65.7	47.2
	CrossFormer-B	7	8	7	4	22.8G	62.1M	389.0G	46.2	67.8	49.5
	CrossFormer-B [‡]	14	16	14	8	20.2G	62.1M	379.0G	46.1	67.7	49.0
Mask-RCNN 1× schedule	CrossFormer-S	7	8	7	4	15.5G	50.2M	301.0G	45.4	68.0	49.7
	CrossFormer-S [‡]	14	16	14	8	12.7G	50.2M	291.1G	45.0	67.9	49.1
	CrossFormer-B	7	8	7	4	23.8G	71.5M	407.9G	47.2	69.9	51.8
	CrossFormer-B [‡]	14	16	14	8	21.0G	71.5M	398.1G	47.1	69.9	52.0

Table 9: Semantic segmentation results on ADE20K validation set with semantic FPN or UPerNet as heads.

Backbone	G_1	I_1	G_2	I_2	Semantic FPN (80K iterations)				UPerNet (160K iterations)				
					Memory	#Params	FLOPs	IOU	Memory	#Params	FLOP	IOU	MS IOU
CrossFormer-S	7	8	7	4	20.9G	34.3M	220.7G	46.0	—	62.3M	979.5G	47.6	48.4
CrossFormer-S [‡]	14	16	14	8	20.9G	34.3M	209.8G	46.4	14.6G	62.3M	968.5G	47.4	48.2
CrossFormer-B	7	8	7	4	14.6G	55.6M	331.0G	47.7	15.8G	83.6M	1089.7G	49.7	50.6
CrossFormer-B [‡]	14	16	14	8	14.6G	55.6M	320.1G	48.0	15.8G	83.6M	1078.8G	49.2	50.1
CrossFormer-L	7	8	7	4	25.3G	95.4M	497.0G	48.7	18.1G	125.5M	1257.8G	50.4	51.4
CrossFormer-L [‡]	14	16	14	8	25.3G	95.4M	482.7G	49.1	18.1G	125.5M	1243.5G	50.5	51.4

ers on both IOU (e.g., 46.4 vs. 46.0) and FLOPs (e.g., 209.8G vs. 220.7G). When taking UPerNet as the segmentation head, a smaller (G, I) achieves higher performance like object detection.

REFERENCES

- Lei Jimmy Ba, Jamie Ryan Kiros, and Geoffrey E. Hinton. Layer normalization. *CoRR*, abs/1607.06450, 2016.
- Tom B. Brown, Benjamin Mann, Nick Ryder, Melanie Subbiah, Jared Kaplan, Prafulla Dhariwal, Arvind Neelakantan, Pranav Shyam, Girish Sastry, Amanda Askell, Sandhini Agarwal, Ariel Herbert-Voss, Gretchen Krueger, Tom Henighan, Rewon Child, Aditya Ramesh, Daniel M. Ziegler, Jeffrey Wu, Clemens Winter, Christopher Hesse, Mark Chen, Eric Sigler, Mateusz Litwin, Scott Gray, Benjamin Chess, Jack Clark, Christopher Berner, Sam McCandlish, Alec Radford, Ilya Sutskever, and Dario Amodei. Language models are few-shot learners. In *Neural Information Processing Systems, NeurIPS*, 2020.
- Chun-Fu Chen, Quanfu Fan, and Rameswar Panda. Crossvit: Cross-attention multi-scale vision transformer for image classification. *CoRR*, abs/2103.14899, 2021a.
- Chun-Fu Chen, Rameswar Panda, and Quanfu Fan. Regionvit: Regional-to-local attention for vision transformers. *CoRR*, abs/2106.02689, 2021b.
- Kai Chen, Jiaqi Wang, Jiangmiao Pang, Yuhang Cao, Yu Xiong, Xiaoxiao Li, Shuyang Sun, Wansen Feng, Ziwei Liu, Jiarui Xu, Zheng Zhang, Dazhi Cheng, Chenchen Zhu, Tianheng Cheng, Qijie Zhao, Buyu Li, Xin Lu, Rui Zhu, Yue Wu, Jifeng Dai, Jingdong Wang, Jianping Shi, Wanli Ouyang, Chen Change Loy, and Dahua Lin. MMDetection: Open mmlab detection toolbox and benchmark. *arXiv preprint arXiv:1906.07155*, 2019.
- Xiangxiang Chu, Zhi Tian, Yuqing Wang, Bo Zhang, Haibing Ren, Xiaolin Wei, Huaxia Xia, and Chunhua Shen. Twins: Revisiting spatial attention design in vision transformers. *CoRR*, abs/2104.13840, 2021.
- MMSegmentation Contributors. MMSegmentation: Openmmlab semantic segmentation toolbox and benchmark, 2020.

-
- Ekin Dogus Cubuk, Barret Zoph, Jon Shlens, and Quoc Le. Randaugment: Practical automated data augmentation with a reduced search space. In *Neural Information Processing Systems, NeurIPS*, 2020.
- Jacob Devlin, Ming-Wei Chang, Kenton Lee, and Kristina Toutanova. BERT: pre-training of deep bidirectional transformers for language understanding. In *Conference of the North American Chapter of the Association for Computational Linguistics, NAACL*, pp. 4171–4186, 2019.
- Alexey Dosovitskiy, Lucas Beyer, Alexander Kolesnikov, Dirk Weissenborn, Xiaohua Zhai, Thomas Unterthiner, Mostafa Dehghani, Matthias Minderer, Georg Heigold, Sylvain Gelly, Jakob Uszkoreit, and Neil Houlsby. An image is worth 16x16 words: Transformers for image recognition at scale. In *International Conference on Learning Representations, ICLR*, 2021.
- Kai Han, An Xiao, Enhua Wu, Jianyuan Guo, Chunjing Xu, and Yunhe Wang. Transformer in transformer. *CoRR*, abs/2103.00112, 2021.
- Kaiming He, Georgia Gkioxari, Piotr Dollár, and Ross B. Girshick. Mask R-CNN. In *International Conference on Computer Vision, ICCV*, pp. 2980–2988, 2017.
- Gao Huang, Yu Sun, Zhuang Liu, Daniel Sedra, and Kilian Q. Weinberger. Deep networks with stochastic depth. In Bastian Leibe, Jiri Matas, Nicu Sebe, and Max Welling (eds.), *European Conference on Computer Vision, ECCV*, volume 9908, pp. 646–661, 2016.
- Zilong Huang, Youcheng Ben, Guozhong Luo, Pei Cheng, Gang Yu, and Bin Fu. Shuffle transformer: Rethinking spatial shuffle for vision transformer. *CoRR*, abs/2106.03650, 2021.
- Diederik P. Kingma and Jimmy Ba. Adam: A method for stochastic optimization. In *International Conference on Learning Representations, ICLR*, 2015.
- Alexander Kirillov, Ross B. Girshick, Kaiming He, and Piotr Dollár. Panoptic feature pyramid networks. In *Conference on Computer Vision and Pattern Recognition, CVPR*, pp. 6399–6408, 2019.
- Hezheng Lin, Xing Cheng, Xiangyu Wu, Fan Yang, Dong Shen, Zhongyuan Wang, Qing Song, and Wei Yuan. CAT: cross attention in vision transformer. *CoRR*, abs/2106.05786, 2021.
- Tsung-Yi Lin, Michael Maire, Serge J. Belongie, James Hays, Pietro Perona, Deva Ramanan, Piotr Dollár, and C. Lawrence Zitnick. Microsoft COCO: common objects in context. In *European Conference on Computer Vision, ECCV*, volume 8693, pp. 740–755, 2014.
- Tsung-Yi Lin, Priya Goyal, Ross B. Girshick, Kaiming He, and Piotr Dollár. Focal loss for dense object detection. *Transactions on Pattern Analysis and Machine Intelligence, PAMI*, 42(2):318–327, 2020.
- Yun Liu, Guolei Sun, Yu Qiu, Le Zhang, Ajad Chhatkuli, and Luc Van Gool. Transformer in convolutional neural networks. *CoRR*, abs/2106.03180, 2021a.
- Ze Liu, Yutong Lin, Yue Cao, Han Hu, Yixuan Wei, Zheng Zhang, Stephen Lin, and Bain-ing Guo. Swin transformer: Hierarchical vision transformer using shifted windows. *CoRR*, abs/2103.14030, 2021b.
- Vinod Nair and Geoffrey E. Hinton. Rectified linear units improve restricted boltzmann machines. In Johannes Fürnkranz and Thorsten Joachims (eds.), *International Conference on Machine Learning, ICML*, pp. 807–814, 2010.
- Zizheng Pan, Bohan Zhuang, Jing Liu, Haoyu He, and Jianfei Cai. Scalable visual transformers with hierarchical pooling. *CoRR*, abs/2103.10619, 2021.
- Olga Russakovsky, Jia Deng, Hao Su, Jonathan Krause, Sanjeev Satheesh, Sean Ma, Zhiheng Huang, Andrej Karpathy, Aditya Khosla, Michael S. Bernstein, Alexander C. Berg, and Fei-Fei Li. Imagenet large scale visual recognition challenge. *International Journal of Computer Vision, IJCV*, 2015.

-
- Peter Shaw, Jakob Uszkoreit, and Ashish Vaswani. Self-attention with relative position representations. In *Conference of the North American Chapter of the Association for Computational Linguistics: Human Language Technologies, NAACL*, pp. 464–468, 2018.
- Aravind Srinivas, Tsung-Yi Lin, Niki Parmar, Jonathon Shlens, Pieter Abbeel, and Ashish Vaswani. Bottleneck transformers for visual recognition. In *Conference on Computer Vision and Pattern Recognition, CVPR*, 2021.
- Hugo Touvron, Matthieu Cord, Matthijs Douze, Francisco Massa, Alexandre Sablayrolles, and Hervé Jégou. Training data-efficient image transformers & distillation through attention. In *International Conference on Machine Learning, ICML*, volume 139, pp. 10347–10357, 2021.
- Ashish Vaswani, Noam Shazeer, Niki Parmar, Jakob Uszkoreit, Llion Jones, Aidan N. Gomez, Lukasz Kaiser, and Illia Polosukhin. Attention is all you need. In *Neural Information Processing Systems, NeurIPS*, pp. 5998–6008, 2017.
- Wenhai Wang, Enze Xie, Xiang Li, Deng-Ping Fan, Kaitao Song, Ding Liang, Tong Lu, Ping Luo, and Ling Shao. Pyramid vision transformer: A versatile backbone for dense prediction without convolutions. *CoRR*, abs/2102.12122, 2021.
- Haiping Wu, Bin Xiao, Noel Codella, Mengchen Liu, Xiyang Dai, Lu Yuan, and Lei Zhang. Cvt: Introducing convolutions to vision transformers. *CoRR*, abs/2103.15808, 2021.
- Tete Xiao, Yingcheng Liu, Bolei Zhou, Yuning Jiang, and Jian Sun. Unified perceptual parsing for scene understanding. In *European Conference on Computer Vision, ECCV*, volume 11209, pp. 432–448, 2018.
- Li Yuan, Yunpeng Chen, Tao Wang, Weihao Yu, Yujun Shi, Francis E. H. Tay, Jiashi Feng, and Shuicheng Yan. Tokens-to-token vit: Training vision transformers from scratch on imagenet. *CoRR*, abs/2101.11986, 2021.
- Sangdo Yun, Dongyoon Han, Sanghyuk Chun, Seong Joon Oh, Youngjoon Yoo, and Junsuk Choe. Cutmix: Regularization strategy to train strong classifiers with localizable features. In *International Conference on Computer Vision, ICCV*, pp. 6022–6031, 2019.
- Hongyi Zhang, Moustapha Cissé, Yann N. Dauphin, and David Lopez-Paz. mixup: Beyond empirical risk minimization. In *International Conference on Learning Representations, ICLR*, 2018.
- Pengchuan Zhang, Xiyang Dai, Jianwei Yang, Bin Xiao, Lu Yuan, Lei Zhang, and Jianfeng Gao. Multi-scale vision longformer: A new vision transformer for high-resolution image encoding. *CoRR*, abs/2103.15358, 2021a.
- Qing-Long Zhang and Yubin Yang. Rest: An efficient transformer for visual recognition. *CoRR*, abs/2105.13677, 2021.
- Zizhao Zhang, Han Zhang, Long Zhao, Ting Chen, and Tomas Pfister. Aggregating nested transformers. *CoRR*, abs/2105.12723, 2021b.
- Zhun Zhong, Liang Zheng, Guoliang Kang, Shaozi Li, and Yi Yang. Random erasing data augmentation. In *Association for the Advancement of Artificial Intelligence, AAAI*, pp. 13001–13008, 2020.
- Bolei Zhou, Hang Zhao, Xavier Puig, Sanja Fidler, Adela Barriuso, and Antonio Torralba. Scene parsing through ADE20K dataset. In *Conference on Computer Vision and Pattern Recognition, CVPR*, pp. 5122–5130, 2017.